ELSEVIER
Earth and Planetary Science Letters 6075 (2001) 1–19
EPSL
www.elsevier.com/locate/epsl

Magnetochronology of the Upper Cenozoic strata in the Southwestern Chinese Tian Shan: rates of Pleistocene folding and thrusting

Jie Chen [a,*], D.W. Burbank [b], K.M. Scharer [c], E. Sobel [d], Jinhui Yin [a], C. Rubin [e], Ruibin Zhao [f]

[a] *Laboratory of Geochronology, Institute of Geology, China Seismological Bureau, Beijing 100029, PR China*
[b] *Department of Geological Sciences, University of California, Santa Barbara, CA 93106, USA*
[c] *Department of Geological Sciences, University of Oregon, Eugene, OR 97403, USA*
[d] *Institut für Geowissenschaften, Universität Potsdam, Potsdam, Germany*
[e] *Department of Geological Sciences, Central Washington University, Ellensburg, WA 98926, USA*
[f] *Xinjiang Seismological Bureau, Urumqi 830011, PR China*

Received 23 August 2001; received in revised form 6 November 2001; accepted 13 November 2001

Abstract

The southwestern Chinese Tian Shan of Central Asia is an actively deforming part of the Indian–Asian collision system. Paleomagnetic investigations of two Plio–Pleistocene terrestrial successions provide the first detailed magnetostratigraphy for the upper Cenozoic strata in this region. Paleomagnetic samples were collected from 358 sites within the Atushi Formation and Xiyu Formation across the Atushi–Talanghe anticline near Atushi. Thermal demagnetization behavior, reversal and fold tests of paleomagnetic stability indicate that the characteristic remanence directions were acquired before tilting and folding of the strata. A composite magnetostratigraphic section for this sequence correlates with the Mammoth subchron to the Jaramillo subchron, between 3.3 and 1.07 Myr, of the geomagnetic polarity timescale of Cande and Kent [J. Geophys. Res. 100 (1995) 6093–6095]. The mean declination ($349 \pm 3°$) in the Boguzihe section indicates a counterclockwise vertical-axis rotation ($-11 \pm 2°$) during the past 1.4 Myr. The conglomeratic Xiyu Formation is time-transgressive along its progradational contact with the underlying Atushi Formation across a map distance of $\sim$6 km, the basal contact ranges from less than 1.0 Myr in the Ganhangou section to 1.9 Myr in the Boguzihe section to the southwest, and to $\sim$2.8 Myr on the northwest limb of the anticline. Northeastward lateral propagation and growth of the Atushi–Talanghe anticline initiated at $\sim$1.4 Myr in the Boguzihe, and $\sim$1.2 Myr in the Ganhangou. The cross section in the Boguzihe provides a conservative (maximum) estimate of shortening rate of $\sim$3.3 (4.4) mm/yr and uplift rate of $\sim$3 mm/yr. This rate represents about half of the geodetically determined shortening rate between the northern Tarim Basin and the Kyrgyz Tian Shan [Wang et al., Acta Seismol. Sin. 22 (2000) 263–270; Reiger et al., Earth Planet. Sci. Lett. 191 (2001) 157–165]. During fold growth over the past 1.4 Myr, the crest of the Atushi–Talanghe anticline eroded at an average rate of 2.6–2.7 mm/yr.

* Corresponding author. Tel.: +86-10-62009149; Fax: +86-10-62009003.
E-mail addresses: chenjieeq@263.net (J. Chen), burbank@crustal.ucsb.edu (D.W. Burbank), kscharer@yahoo.com (K.M. Scharer), sobel@rz.uni-potsdam.de (E. Sobel), charlier@geology.cwu.edu (C. Rubin).

0012-821X/01/$ – see front matter © 2001 Published by Elsevier Science B.V.
PII: S0012-821X(01)00579-9

Keywords: Late Cenozoic strata; magnetostratigraphy; Pleistocene folding; rates; southwestern Chinese Tian Shan

1. Introduction

Late Cenozoic deformation in the Tian Shan of Central Asia is the result of the continued northward indentation of India into Eurasia. The late Cenozoic terrestrial sequences in central Asia principally comprise prisms of sediment shed into foreland basins during Miocene–Pleistocene times from the actively deforming ranges of the Indo–Asian orogen (e.g. [1–7]). With thicknesses often exceeding several kilometers, these foreland strata hold great potential for documenting the tectonic and erosional histories of the adjacent ranges. In order to exploit this sedimentary record to its fullest it is necessary to have reliable chronologic control that delineates the timing of events and rates of processes. Such temporal data provide a critical context for understanding the interplay between mountain building, erosion, deposition, and climate. In the mountains of Central Asia, for example, the Plio–Pleistocene was a time of dramatic change, as thrusting increasingly impinged on the proximal forelands, glaciers expanded and contracted, boulder-rich aprons of debris were shed into most basins, and rates of deposition increased in many basins [8,9]. Yet, these very changes and the resultant upward coarsening of grain sizes during late Cenozoic times often render it difficult to obtain reliable chronologies, especially as few fossils are preserved in the coarse, terrestrial successions, and volcanic ash is uncommon.

Magnetic polarity stratigraphy, supported by biostratigraphic evidence and fission-track ages from volcanic tuffs, has been successfully applied as a geochronologic method in the Siwalik Group and its temporal equivalents in the Indo–Gangetic foreland (e.g. [10–14]), where it has provided the temporal context for interpreting the detrital record of the Himalayan orogen. In the Chinese Tian Shan, however, the magnetostratigraphy of the upper Cenozoic strata has been much less studied, owing in part to the relative remoteness of these sections and the common absence of volcanic ash beds that may serve to constrain interpretations of the magnetostratigraphy. Several studies of these upper Cenozoic strata in the Chinese Tian Shan have produced magnetostratigraphies (e.g. [15–18]), but the results have commonly been ambiguous due to unreliable radiometric dates and issues related to demagnetization, the brevity or incompleteness of the magnetostratigraphic record, poor biostratigraphic control, or uncertain field correlations.

The aim of this paper is to report new paleomagnetic results from the Plio–Pleistocene strata of the southwestern Chinese Tian Shan from localities near Atushi (Fig. 1). We describe a detailed magnetostratigraphic study of a well-exposed, >3000-m-thick section of late Cenozoic strata. Based on analysis of 358 paleomagnetic sites, the succession of documented reversals permits a clear correlation to the magnetic polarity time scale [19], thereby providing accurate ages for this sequence, dating the initiation and estimating shortening rates of the late Cenozoic folding and thrusting in this region. In addition, we hope that our study will establish a chronologic template for future studies in this region.

2. Geologic setting

2.1. Tectonic setting

The east–west-trending Tian Shan extend >2500 km across central Asia, and bound the northern margin of the Tarim Basin (inset in Fig. 1). The present topography of the Tian Shan was created during Cenozoic times as a result of the India–Asia collision [2,17,22]. Up to 9 km of Cenozoic sediments have accumulated along the southwestern margin of the Tian Shan, and these sediments have been folded into a suite of elongate anticlines and synclines [4,22–24]. This deformation zone contains two remarkable, oppositely vergent arcuate fold-and-thrust systems (Kepingtage–Yishlakekalawuer and Ka-

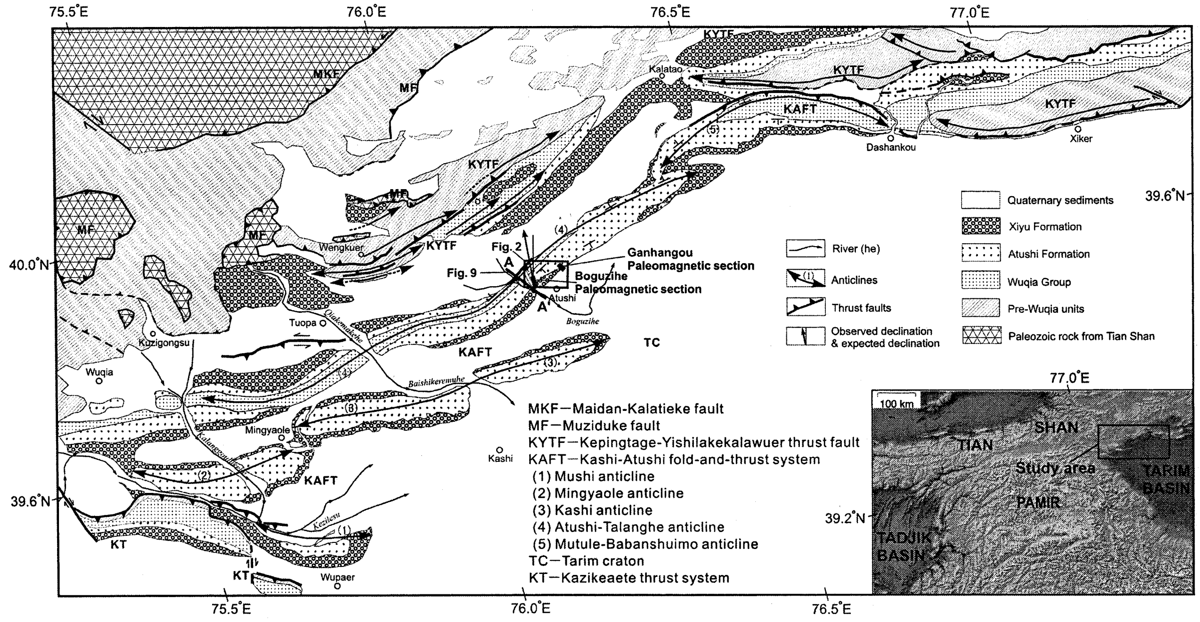

Fig. 1. Simplified geologic map of the northwestern Tarim Basin, southwestern Chinese Tian Shan (based on our field mapping and interpretation of Landsite TMs and aerial photos; XBGMR [20]; and Wang et al. [21]), showing the localities of paleomagnetic sampling sections.

shi–Atushi fold-and-thrust zones) extending from east of Keping to west of Kashi. Paleozoic to Cenozoic strata are involved in this deformation [22,24]. Thrusting and folding on the Kashi–Atushi fold-and-thrust system are presently north-vergent, overriding older Cenozoic south-vergent structures, and consist of five en echelon anticlines (Fig. 1): the Mushi, Mingyaole, Kashi, Atushi–Talanghe and Mutule–Bapanshuimo anticlines. Our study focused on the Atushi–Talanghe anticline. These anticlines represent north-vergent detachment folds that developed during late Cenozoic times and are interpreted to have accommodated much of the recent shortening that has been shown geodetically to occur south of southern Kyrgyzstan [25,26]. Because these strata have not been deformed by earlier orogenies, they provide a pristine succession within which to discern the style, age, and rates of shortening.

All of these anticlines are composed of two distinct tectonostratigraphic sequences that either predate or are synchronous with folding [24,27]. The lower pre-growth strata are predominantly concordant, display uniform dip panels, and define the large-scale geometry of the anticline. In contrast, the upper growth strata record the initiation and progression of folding, as evidenced by progressively less tilted beds and syntectonic unconformities.

2.2. *Pliocene–Pleistocene lithostratigraphy, biostratigraphy, and sedimentology*

2.2.1. *Lithostratigraphy and biostratigraphy*

The nomenclature of the Tertiary stratigraphic units used in this study follows that of Zhou and Chen [28], who, on the basis of biostratigraphic and lithostratigraphic considerations, divided the Tertiary strata into a dominantly marine lower Tertiary sequence and a dominantly nonmarine upper Tertiary sequence. The upper Tertiary sequence comprises 5000–8000 m of terrestrial clastic sediments within the western Tarim Basin and is composed of the Wuqia Group (Keziluoyi, Anjuan and Pakabulake Formations) and the Atushi and Xiyu Formations. The Wuqia Group is characterized by multi-colored mudstones, siltstones, sandstones, interbedded with gypsum and gypsiferous claystones. These rocks are interpreted to be Late Oligocene–Miocene in age – a claim based on their foraminifera fauna [20,27,29]. The Atushi Formation consists of gray-yellow, tan medium-grained sandstone and sandy mudstone with thin layers of fine gravel. The age of the Atushi Formation is poorly constrained and interpreted to be Pliocene, a claim based mostly on charophyte and Ostracoda [20,27,28].

The overlying Xiyu Formation is dominated by massive pebble-to-boulder conglomerate typical of the channel and debris-flow deposits of alluvial fans. The Xiyu Formation is widely distributed along the margins of the Tian Shan, and has been assigned both the Pliocene and early Pleistocene with a great deal of uncertainty in the claims (e.g. [3,15,16,20,27,30]). The only chronostratigraphic control is provided by *Equus sanmeniensis*, interpreted to be early Pleistocene in age [15,21]. It occurs at the transition zone between the Dushanzi Formation (equivalent to Atushi Formation) and the Xiyu Formation at Anjihai, northern Chinese Tian Shan [7]. It has been claimed that a correlation can be drawn between the formation of the northern Tian Shan and those of the study area [30]. However, given the distance involved and the nature of the depositional environments, such a claim must be seen as tentative.

Due to the lack of biostratigraphic constraints specific to the study site, the commonly assigned age of the Xiyu Formation is based on lithostratigraphic correlations from the adjoining region (e.g. conglomerate = Xiyu Formation = Pleistocene) [3,7,20,31]. As a result, many authors have assumed that the conglomerate exposed along the margins of the Tian Shan represents synchronous deposition (e.g. [7,31]) and indicates a late Plio–Pleistocene initiation of deformation (e.g. [3]). As shown below, any claim for synchronous deposition of the upper Cenozoic conglomerate is erroneous.

The Boguzihe section (named after a river which dissects the Atushi–Talanghe anticline) is located in a generally N–S-trending outcrop belt defining the southeastern limb of the Atushi–Talanghe anticline (Figs. 1 and 2). At this site, Tertiary strata in the southeastern limb of the Atushi–Talanghe anticline are >3500 m thick and are exposed in an unfaulted southeast-dipping ($\sim 55°$) homocline. The 1600-m-thick section measured during this study begins ca. 1400 m (stratigraphically) above the top of the Pakabulake Formation and can be divided (from oldest to youngest) into two distinct lithostratigraphic packages (Figs. 1 and 3). On the basis of regional lithostratigraphic correlation, the lower unit of the measured section is equivalent to the Atushi Formation, whereas the upper unit (Fig. 3) represents the Xiyu Formation [27]. The other measured section used in this study is the Ganhangou section. The section is 815 m thick, is located ~ 6 km east of the Boguzihe section (Fig. 2), and includes the upper part of the Atushi Formation. No fossils were found in either section. However, ~ 8 km to the south of the Boguzihe section in the Kashi anticline and ~ 70 km to the east in the Kepingtage anticline, Zhou and Chen [20,28] found *Ilyocypris evidens* Mandelstam, *I. errabundis* Mandelstam, *I. manasensis* Mandelstam, *Candoniella albicans* (Brady), *Eucypris* sp., *Candoniella* sp., *Eucypris concinna* Schneider, *Potamocypris reflexa* Schneider, *Cypris* sp., *Limnocythere angulata* Mandelstam, *L. luculenta* Livental, *Candona* aff. *rostrata* Brady and Norman, *Darwinula* sp., *Charites* cf. *sadleri*, *Grambastichara tornata* throughout the correlative stratigraphic interval in the Atushi Formation. This assemblage has been interpreted by these authors to indicate a Pliocene age, and it is this assemblage which pro-

→

Fig. 2. (a) An enlarged aerial photo view of two paleomagnetic sampling sections. Normal (reversed) sites depicted as closed (open) circles. Note that the lower Xiyu conglomerate interfingers laterally with the Atushi Formation, and occurs as focused lenses of conglomeratic strata bounded on either side by finer-grained strata. (b) The sampling routes along the Boguzihe with locations of the 314 sampling sites/levels (B1–B285 were collected in 1999, and B318–B300 were collected in 2000) indicated. (c) The sampling routes along the Ganhangou with locations of the 44 sampling sites/levels (G1–G43 were collected in 2000) indicated. For clarity, only selected sites are labeled.

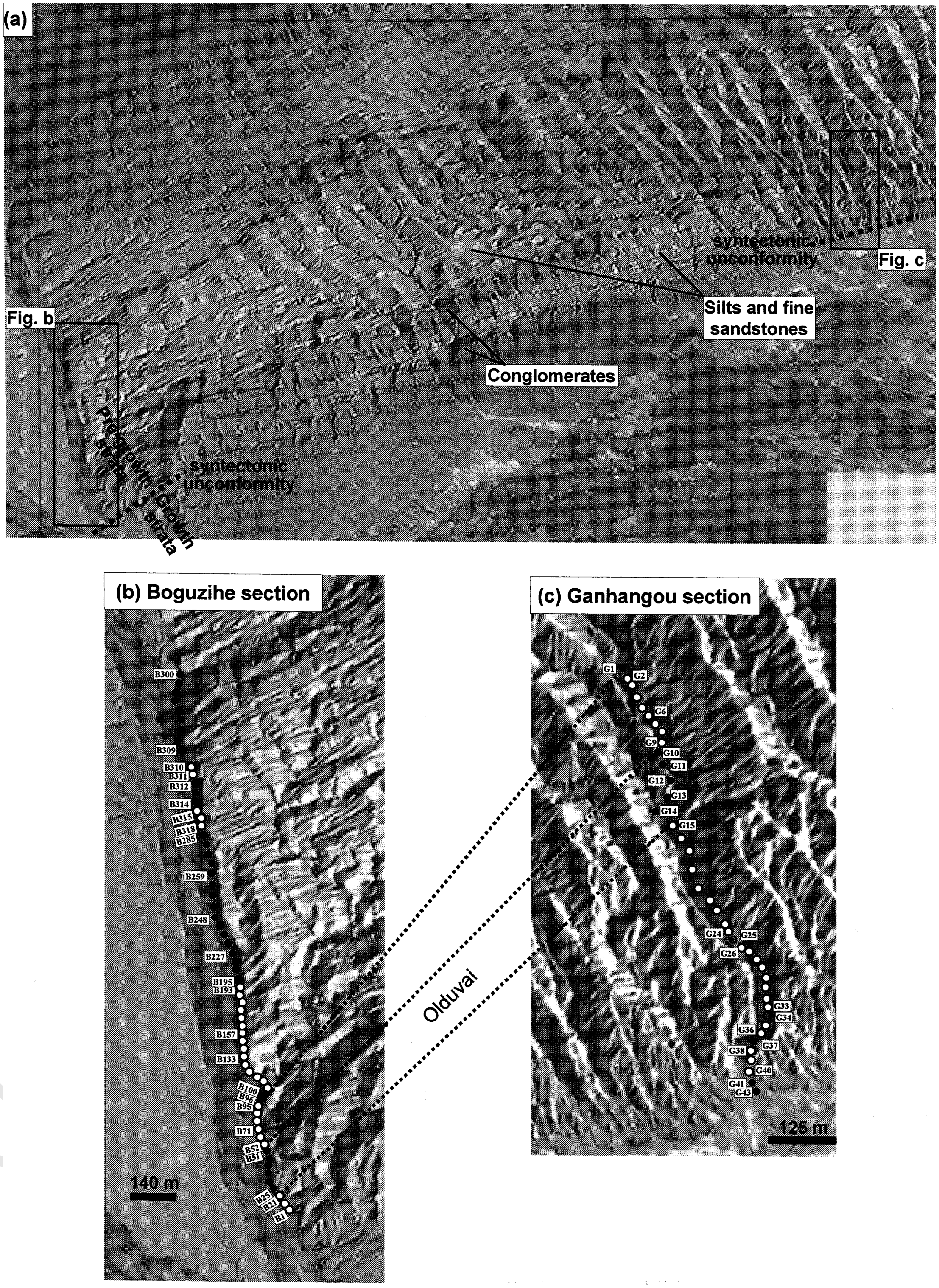
(a)
syntectonic unconformity
Fig. c
Silts and fine sandstones
Conglomerates
Fig. b
Pre-growth strata
Growth strata
syntectonic unconformity
(b) Boguzihe section
140 m
Olduvai
(c) Ganhangou section
125 m

vides the chronostratigraphic control for the present study.

2.2.2. Sedimentology

The Atushi Formation consists of light-gray fluvial sandstones coarsening upwards into yellowish and grayish conglomerates across a thickness of ~1.42 and 0.82 km in the Boguzihe and Ganhangou sections, respectively (Fig. 3). Coarse-grained facies occur as both channelized and sheet sandstones and gravels. The sheet sandstones are commonly 2–3 m thick, whereas the channelized sandstones may attain thicknesses of 8–10 m. Associated fine sediment packages consist of predominantly decimeter-scale beds, which are laterally continuous over tens of meters. In the upper parts of the Atushi Formation, the fine-grained strata decrease in thickness and frequency and are commonly incised up to 2 m by the channelized sandstone and gravel bodies as they become increasingly dominant.

The sandstone and gravel facies include both single- and multi-storied channel sandbodies several meters thick. The medium-grained to granule sandstone includes minor conglomeratic channel fills and is characterized by planar and trough cross-bedding and by numerous reactivation surfaces. Load structures and soft sediment deformation structures are prominent at the base of the channel sandstones. Cross-beds and paleochannel cross-sections indicate a paleoflow direction predominantly towards the east–southeast.

The fine-textured sediments are commonly laminated and display an alternation of thin, fine-sand/silt-mud laminations or fine sands with mud partings. Mudcracks, burrows, and both carbonate and gypsiferous concretions are common. Enclosed fine sandstones may be ripple-laminated. Pedogenic alteration of the fine-grained sediments is minor.

Overall, this coarsening upward megacycle is interpreted as a prograding multi-channel river system that encroached on sand and mud flats associated with ephemeral lakes [32]. Ripple-scale cross-bedded sandstones, laminated and burrowed mudstones with mudcracks are interpreted to represent shallow water to emergent lacustrine environments, whereas the sheet sandstones associated with these facies are interpreted to represent unchannelized flow across lake-marginal mud and sand flats. The channelized sandstones are interpreted to represent either the upstream feeder systems to the lacustrine facies or entrenchment in response to base-level fall. In the upper section, significant grain-size coarsening, a marked decrease in the abundance of fine-grained deposits and a preponderance of superposed conglomeratic sheets are interpreted to represent the progradation of braided rivers across the region.

The boundary between the Atushi and Xiyu Formations is marked by a sudden, qualitative shift in lithology that is easily mapped in the study area (Figs. 2 and 3). With a thickness of >800 m, the Xiyu Formation conformably overlies the Atushi strata. Near its base, pebble-sized gravel beds 0.3–7 m thick alternate with discontinuous, poorly sorted sand lenses with isolated pebbles. Less common are beds with thicknesses of 5–15 m which are matrix-supported; most beds comprise well-rounded, clast-supported gravels. Many of the gravel units are lenticular, and they commonly display a positive correlation of grain size with bed thickness.

Higher in the Xiyu Formation, the gravel beds become both thicker and more massive, whereas the sandstones become thinner and less frequent. The frequency of clast-supported gravels and the maximum clast sizes increase upward in the section. Planar bedding and shallow troughs dominate the gravel bedding, whereas clast imbrication seldom occurs. In the upper third of the section, sandstone beds become scarce.

At a subregional scale, the Xiyu conglomerate is well preserved in 'water gaps' which cut through the southern limb of the anticline. The deposits are locally eroded on the northern limb

→

Fig. 3. Lithology and magnetostratigraphic results from (a) Boguzihe section and (b) Ganhangou section with declination, and VGP (virtual geomagnetic pole) latitude plotted against stratigraphic height and correlation to the GPTS of Cande and Kent [19].

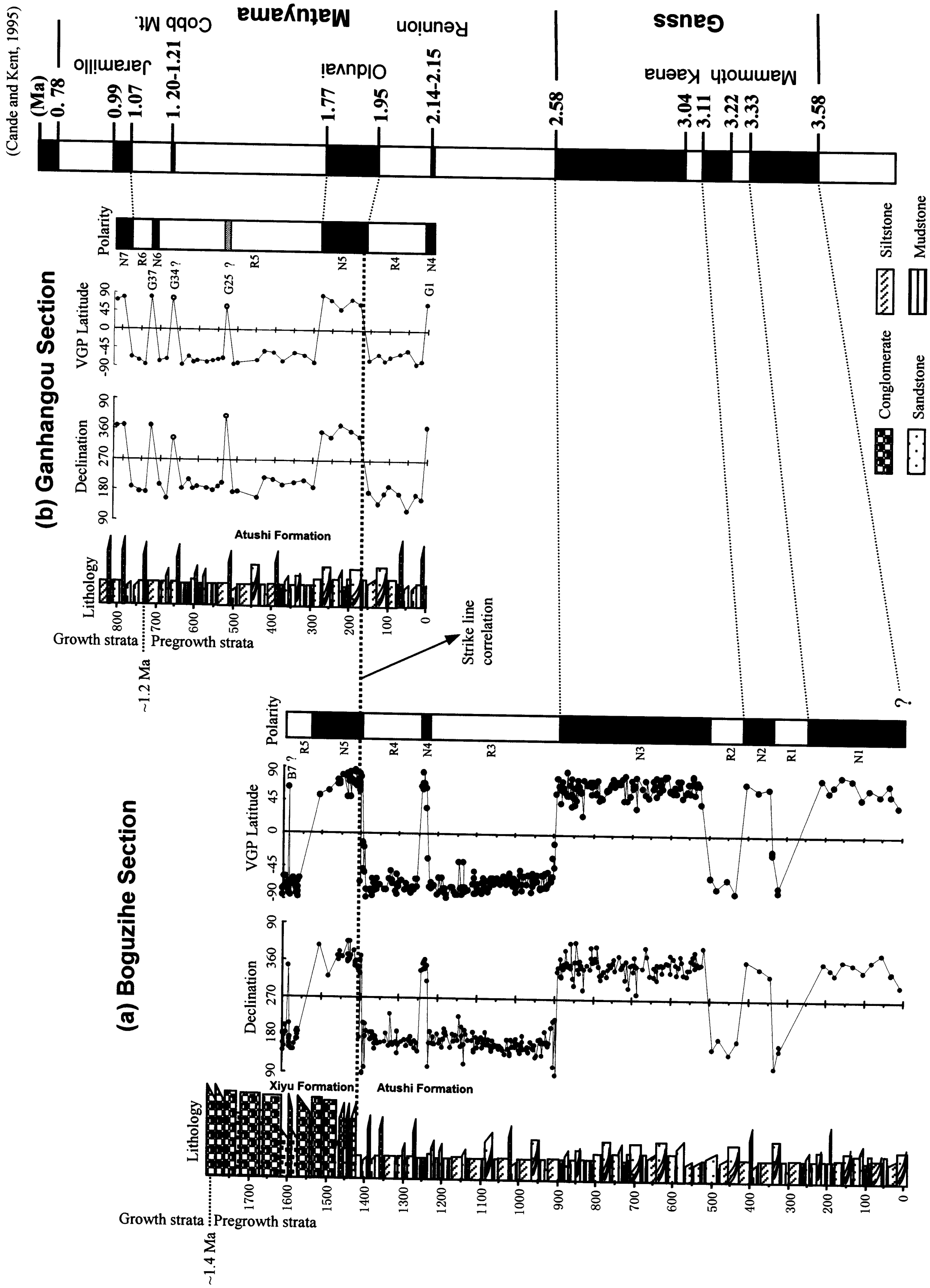
GPTS
(Cande and Kent, 1995)
(Ma)
0.78
0.99
1.07
1.20-1.21
1.77
1.95
2.14-2.15
2.58
3.04
3.11
3.22
3.33
3.58
Jaramillo
Cobb Mt.
Matuyama
Olduvai
Reunion
Gauss
Mammoth
Kaena
(b) Ganhangou Section
Polarity
N7
R6
N6
R5
N5
R4
N4
VGP Latitude
-90 -45 0 45 90
G37
G34 ?
G25 ?
G1
Declination
90 180 270 360 90
Lithology
Atushi Formation
Growth strata
Pregrowth strata
~1.2 Ma
Strike line correlation
(a) Boguzihe Section
R5
N5
R4
N4
R3
N3
R2
N2
R1
N1
B7 ?
Xiyu Formation
Atushi Formation
~1.4 Ma
Conglomerate
Sandstone
Siltstone
Mudstone

of the structure. The outcrop pattern indicates that the Xiyu Formation interfingers laterally with the Atushi Formation (Fig. 2). In its lower parts, the sediments of the Xiyu Formation occur as focused lenses of conglomeratic strata bounded on either side by finer-grained strata. In its upper parts, the Xiyu sediments represent a laterally continuous sheet across most of the landscape.

The Xiyu Formation is interpreted as a high-gradient, multi-channel alluvial river system prograding toward the south. In its early stages, the channel facies were focused into localized zones a few kilometers in width, whereas in the later stages, the alluvial system covered the entire depositional basin. Limited paleocurrent data indicate flow to the south throughout the deposition of the Xiyu Formation.

3. Paleomagnetic sampling, laboratory methods, statistical analysis and results

3.1. Sampling

Detailed magnetostratigraphic studies were undertaken on both sections. The paleomagnetic record for the Boguzihe section begins in the middle Atushi Formation and ends in the lower Xiyu Formation. Coarse sediment facies prohibited further sampling (Fig. 2). Strike-line mapping demonstrates that the succession of the Ganhangou section is stratigraphically equivalent to the Xiyu Formation at Boguzihe; the sediment characteristics, however, are different. The Ganhangou section lacks the coarse conglomerates diagnostic of the Xiyu Formation. The section has sediment characteristics which resemble the finer-grained strata of the upper Atushi Formation (Figs. 2 and 3). The explanation for these differences lies in the respective location of the two sections to the hinterland sources and transport paths of the coarse conglomerates. The top of the Boguzihe paleomagnetic section overlaps the lower $\sim$350 m of the Ganhangou section. Stratigraphic thicknesses were measured with either tape and compass survey or Jacob staff and Abney level. At least two or three oriented cores were drilled at each of 314 sedimentary beds in the Boguzihe section. Sites were spaced 0.5–5 m apart in the middle–upper Atushi Formation and increased to 15–25 m apart in the lower Atushi and Xiyu Formations. Sampling of the top of the preserved section at the Boguzihe section was not possible due to the massive conglomerates of the Xiyu Formation and the scarcity of suitable lithologies. In the Ganhangou section, two or three oriented cores were drilled at each of 44 sites with spacings of 15–30 m. Some variation in site spacing was necessary so as to obtain suitably fine-grained lithologies and to avoid faulted, disturbed, or highly altered sediments.

Sixty-four samples at eight sites were collected at the northern limb of the Atushi–Talanghe anticline along the Boguzihe section and used in a 'fold test'. These eight sites were stratigraphically correlated to the lower part of the Boguzihe paleomagnetic section.

3.2. Measurements

Measurements were made using a computer-controlled, magnetically shielded cryogenic magnetometer with a background noise level of $\sim 5\times10^{-12}$ Am^2, located within a magnetically shielded room at the California Institute of Technology Paleomagnetics Laboratory. At least one specimen per sampling site/level was progressively demagnetized by applying stepwise alternating field (AF) and thermal demagnetization. For sites that yielded ambiguous polarity results or near polarity transition zones that were defined by single sites, an additional two or three specimens were measured. All measured specimens were subjected to both AF and thermal demagnetization. Three steps of AF demagnetization were initially performed on all specimens, usually up to a maximum of 5 or 10 mT. Thermal demagnetization was then used, typically in: (i) 150°C steps up to 300°C, (ii) 100°C or 50°C steps up to 550°C, and (iii) 25°C or 10°C steps up to 680°C or 690°C.

Rock magnetic studies of 38 samples representing the varied lithologies of the Atushi and Xiyu Formations were undertaken in order to define the mineralogy and characteristic magnetic domains of these rocks. As shown in Fig. 4, most of the intensity in the IRM acquisition curves was

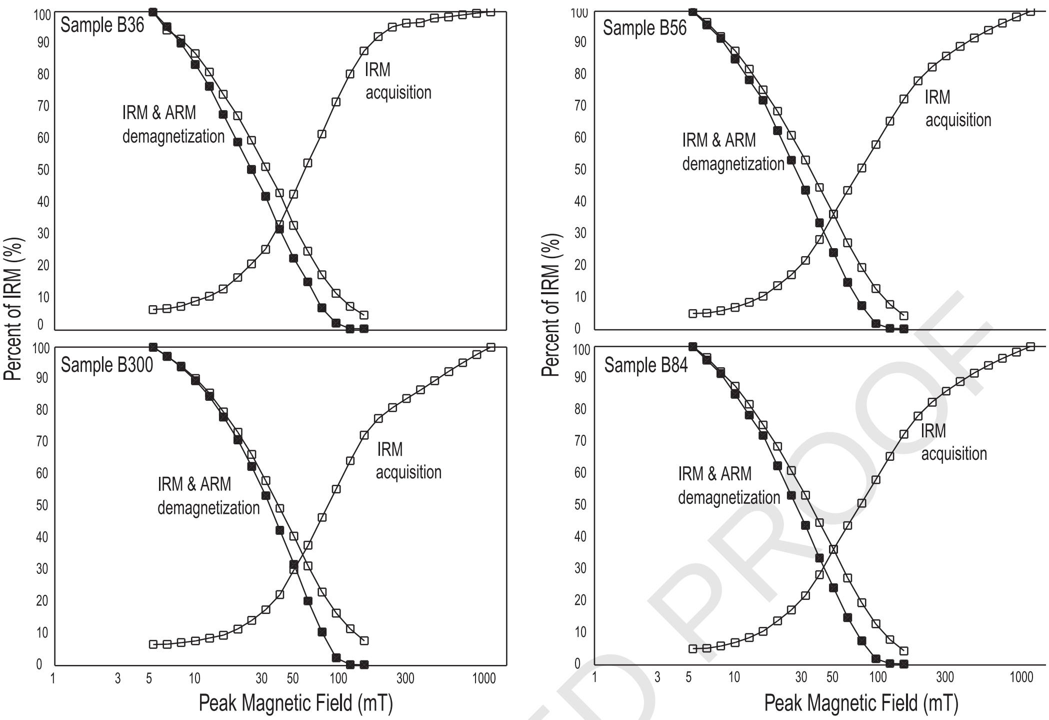

Fig. 4. IRM (isothermal remanent magnetization)/ARM (anhysteretic remanent magnetism) acquisition and demagnetization curves for selected paleomagnetic samples analyzed during this study. Data for the IRM acquisition and AF demagnetization of the IRM are shown with open symbols. The solid symbols show the AF demagnetization of the ARM acquired in a 2 mT direct current biasing field with a 100 mT (max) alternating field.

acquired after exposure to peak fields of less than 300 mT. The slopes of the upper most IRM acquisition curve of the coarse samples (silts and fine sandstones, e.g. B36) are noticeably gentler than that of the fine samples (mudstones and muddy siltstones, e.g. B300). This is indicative of magnetite with a portion of higher coercivity material, such as hematite.

3.3. Paleomagnetic results

3.3.1. Demagnetization

The intensity of the NRM for these specimens was of the order of 10^{-2}–10^{-3} A/m. Progressive demagnetization successfully resolved multiple components of magnetization. Equal area projection and orthogonal vector plots reveal two clear components for the vast majority of the specimens: a high-temperature component (HTC) and a low-temperature component (LTC) (Fig. 5a). The LTC, which is a low-coercivity, low-blocking-temperature component, is removed by AF demagnetization at 5 or 10 mT and thermal demagnetization at 150°C. An equal area plot of the LTC from most specimens (normal, reverse, and transitional) reveals a mean direction (declination: 8°; inclination: 57°), as calculated from Fisher statistics [33], which is very close to the present-day local field. Due to the steep dip of the bedding in these sections, this present-day overprint is easily distinguished from both normal and reversed primary magnetic directions.

With respect to the HTC, we can divide the demagnetization behavior into four categories. Type I (Fig. 6a) shows magnetizations up to 450 or 550°C that cannot be separated from the LTC that lies close to the present local field (PLF). The magnetization became unstable between 500 or 550 and 690°C and was not used. Type II (Fig. 6b) reveals well-defined, two-component magnetizations: a LTC with unblocking temperature to 300°C and a HTC characteristic component with

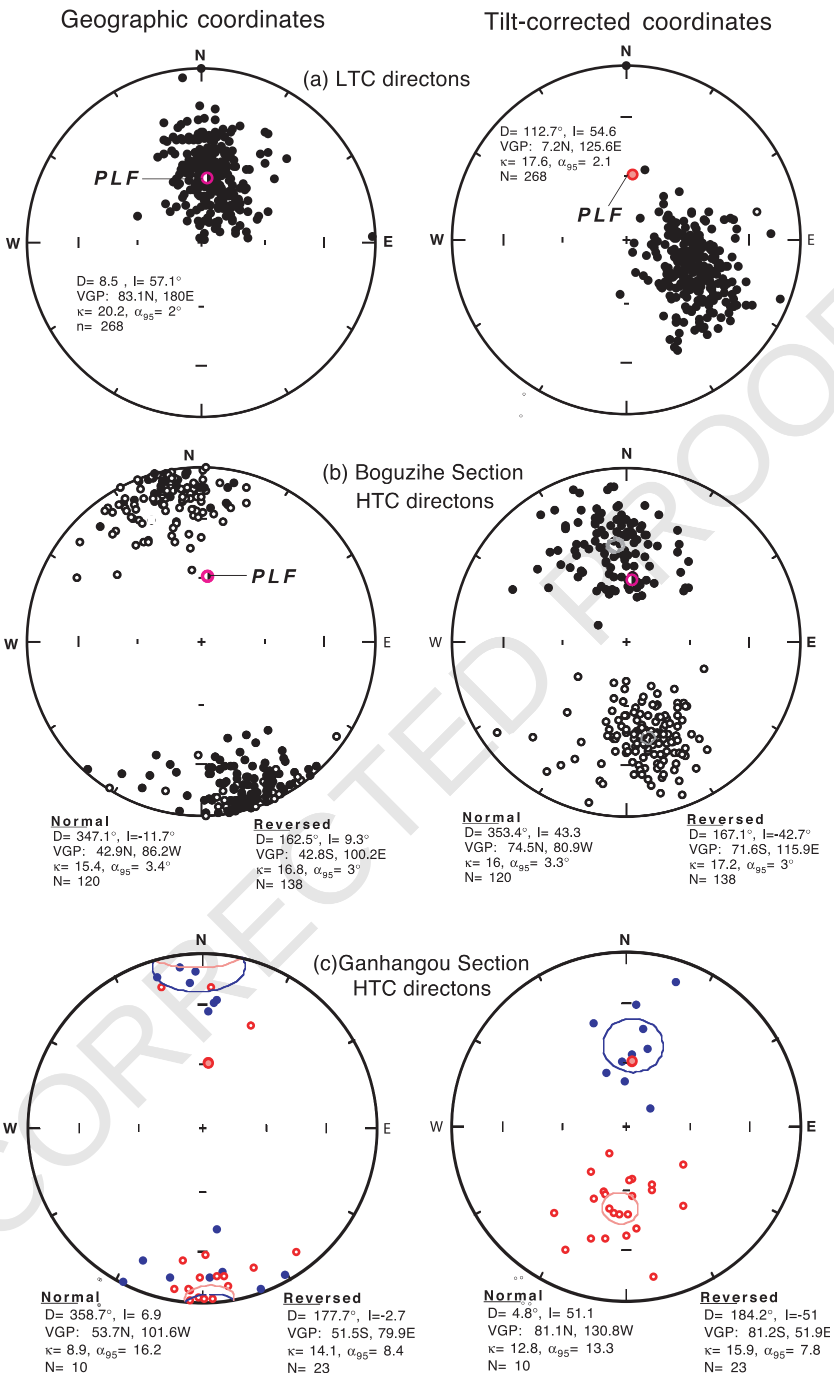

Fig. 5. (a) Stereoplot (equal area projections) of LTC from most of the samples in geographic coordinates. Closed circles and PLF (present local field) represent lower hemisphere projections. The mean direction lies near the present-day field direction for the Boguzihe section (Dg = 8.5°, Ig = 57.1°; VGP: 83.1N, 180E; $k = 20.2$, $\alpha_{95} = 2°$, N = 268°). (b,c) Reversal tests of paleomagnetic stability in the Boguzihe and Ganhangou sections respectively.

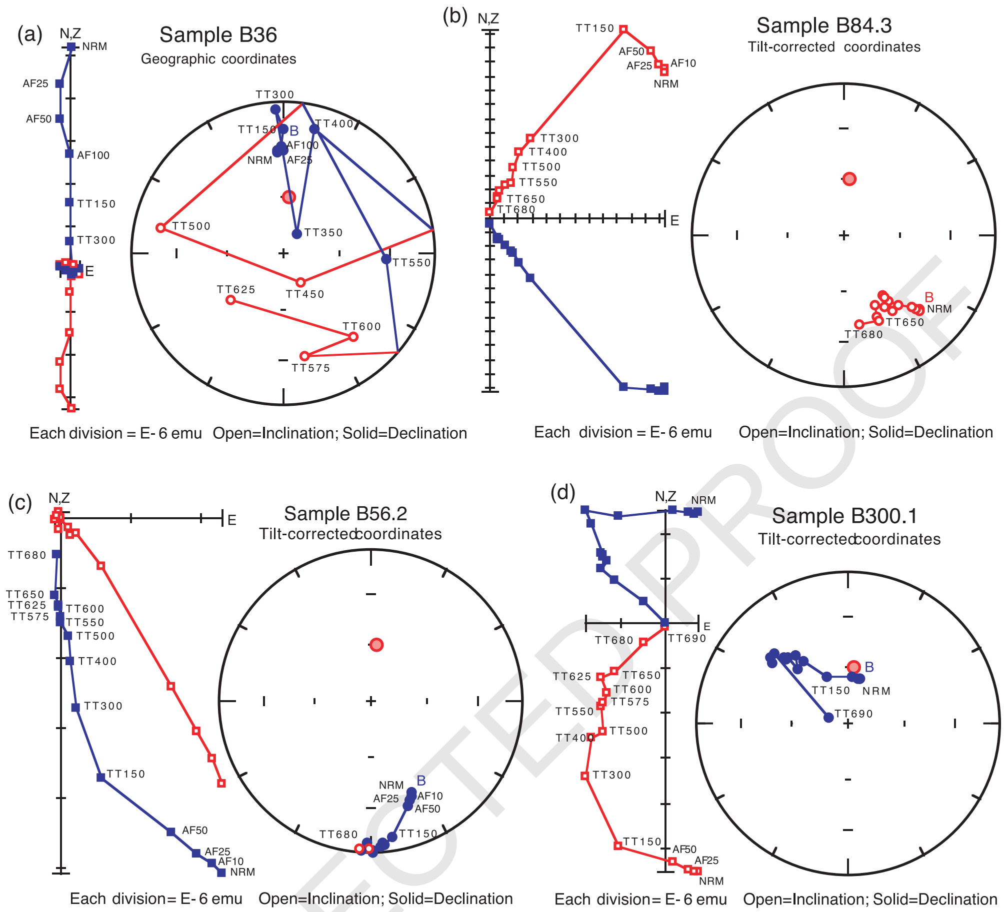

Fig. 6. Representative demagnetization (Zijderveld diagrams and equal-area projections) showing typical thermal demagnetization behavior for (a) an example of a specimen that did not reach a stable, linear demagnetization path (poorly sorted fine-medium sandstone), (b) well-defined, two-component magnetizations, (c) a representative of some specimens showing only a tendency toward a reversed polarity, and (d) specimens with three-component magnetizations. The reversed characteristic remanence direction can easily be distinguished from a present-day overprint due to the steep bedding dips in this study.

both normal and reversed polarities. The vast majority of the specimens possess this type of demagnetization. In type III (Fig. 6c), demagnetization could not be completed, and the endpoints show only a tendency toward a final direction. Comparison of nearby specimens with type II behavior suggests that the HTC is the same in both types II and III. Hence there is only one characteristic component in these specimens. The intersection of great circles, given by the McFadden and McElhinny [34] 'combined line and plane data analysis' method, was used to determine the HTC of type III specimens which could then be used in the computation of site-mean directions. Type IV displays three components (Fig. 6d): a LTC similar to that described above; a secondary component that is revealed between 300°C and 575 or 600°C; and a HTC above 600 or 625°C that carries the characteristic remanence (ChRM) direction.

To determine ChRM directions, principal component analysis [35] was performed for each specimen. Data from a minimum of three, and more typically four to eight, temperature steps were used for least-squares fits, in which the origin of the vector-component diagram was included as an additional datum. Typical maximum angular deviation (MAD) was between 1 and 15°.

3.3.2. Statistical treatment and results

Following determination of specimen ChRM directions, site-mean ChRM directions for sites with more than two specimens were determined using methods of Fisher [34] and examined using the test for randomness of Watson [36]. Sites yielding one or two specimen ChRM directions with MAD < 10° or with three or more specimens yielding ChRM directions that are nonrandom at the 5% significance level and with site-mean 95% confidence limits (α_{95}) < 19° are considered the most reliable results and are designated class A sites. Sites yielding only one specimen ChRM directions with 10≤MAD < 15° or with two or three specimens yielding more dispersed ChRM directions but unambiguous polarity are designated class B sites. In the Boguzihe section, out of 314 sites, 258 sites are class A, 36 sites are class B, and 20 sites yield ambiguous polarity and were rejected. In Ganghangou section, 33 sites out of 44 sites are class A, seven sites are class B, and four sites yield ambiguous results and were rejected.

Tilt corrections improve the grouping of ChRM inclinations significantly when both sections are considered together (Fig. 5b,c). Because both sections display generally steep homoclinal dips, the grouping of site-mean ChRM declinations within individual sections is only slightly improved by tilt corrections.

Two critical tests of the ChRM directions were performed on these sedimentary rocks – a reversal test and a fold test in order to constrain the time of ChRM acquisition. The formulation of McFadden and McElhinny [37] was used to characterize the reversal test. Both sections pass the common distribution test. For the analytical test (assuming identical *k* values), with one mean reversed through the origin, the Boguzihe site means have an observed angular difference of 3.3° and a calculated critical angle (95% confidence level) of 4.4°. Thus, this section passes the analytical test with an 'A' quality classification [37]. For Ganhangou, the observed angular difference is 4.4° with a calculated critical angle (95%

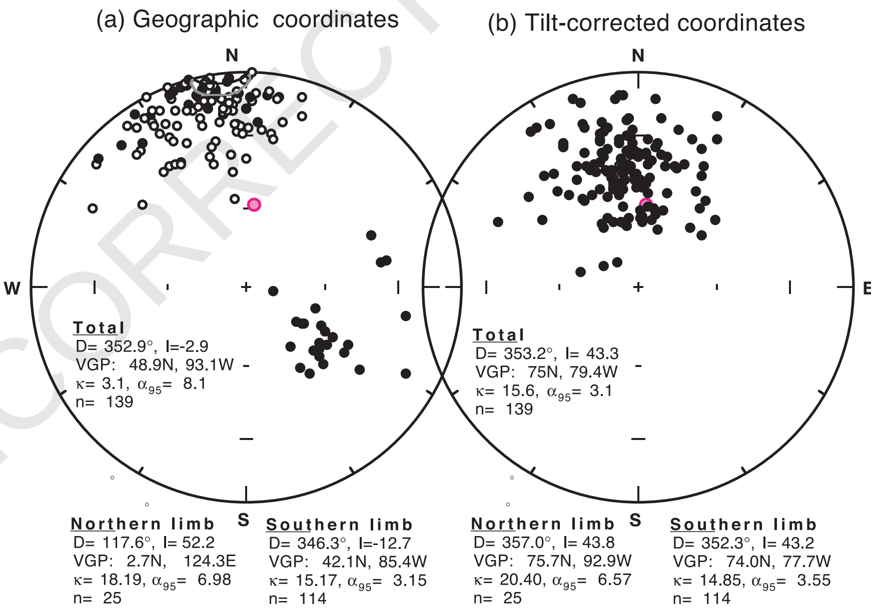

Fig. 7. Fold test of paleomagnetic stability in the Boguzihe section. The fold test reflects the ChRM direction for each sample ($n=139$) taken from sites ($N=120$) on opposing limbs of the Atushi–Talanghe anticline before bedding tilt correction (a) and after bedding tilt correction (b). A significant increase in precision in b relative to a indicates a positive fold test, where the characteristic component of magnetization was acquired before folding.

confidence level) of 14.9° indicates that the section passes a 'C' quality reversal test.

The McFadden and Jones [38] fold test was used to compare ChRM directions from specimens on opposing limbs of the Atushi–Talanghe anticline, before and after tilt correction. Only six class A sites (for a combined 25 class A specimens) out of eight sites (64 specimens) are on the northwestern limb of the anticline. However, the tilt correction produces an increase of k from 3.1 to 15.6 when compared to 114 class A sites from the lower unit of the Boguzihe section at the southeastern limb (Fig. 7). The statistic $f(R) = [(R_a + R_b - R^2/(R_a + R_b))/2(N - R_a - R_b)]$ (where R, R_a and R_b are the lengths of the vector sums of the site-mean directions of all sites ($R = 112.273$), sites from the northwestern limb ($R_a = 5.864$) and from the southeastern limbs ($R_b = 106.416$), with $N = N_a + N_b = 6 + 114 = 120$, respectively) using tilt-correction observations gives 0.001 which is much smaller than the critical value at the 95% probability level, this being 0.0257. This indicates that the fold test is positive at the 95% confidence level and verifies that the sediments in the sections acquired their ChRM directions before tilting and folding of the strata.

The positive results from these two stability tests, along with the fact that stratigraphically bound polarity reversals are contained within the sections, show that these ChRM directions were acquired by the sediments at or soon after deposition.

4. Magnetostratigraphy and correlation to the geomagnetic polarity timescale (GPTS)

Only class A and B site-mean declinations and inclinations were used to calculate virtual geomagnetic pole (VGP) positions. The individual site VGP latitudes were then plotted against stratigraphic height for each of the Boguzihe and Ganhangou sections, resulting in a magnetic polarity sequence for the middle and upper parts of the Atushi Formation and Xiyu Formation (Fig. 3). With few exceptions, each polarity zone in our magnetic stratigraphy is defined by two or more paleomagnetic sites. Only one normal polarity zone at the top of the Boguzihe section is defined by one site – B7 (Fig. 3). Because this polarity zone was only defined by one site, for which only one specimen was measured, the result was not used. For sites below and above the sampling horizon for B7, more than two specimens with subparallel reversed polarity directions were available. Four polarity zones in the Ganhangou section are defined by one site each (sites G1, G25, G34, G37), with each site containing more than three specimens. Sites G1, G25, and G37 are class A sites. Site G34 yielded a ChRM direction with $\alpha_{95} = 29.3°$ and was rejected.

The age range of the measured sequences is generally considered to be between 1 and 5 Myr, based on regional lithostratigraphic correlation and limited fossil evidence in adjacent sections [27,28]. Unfortunately, no fossils were found in our sections that would provide more rigorous biostratigraphic age constraints. Strike-line mapping from aerial photos clearly demonstrates the stratigraphic correlation between the two sections (Figs. 2 and 3). The sharing of magnetozones N4, R4, N5, and R5 in both the Boguzihe section and the Ganhangou section provides a firm correlation between the two sections.

In the absence of biostratigraphic control specific to the sections studied, we tentatively refer the obtained magnetic polarity sequence with the GPTS of Cande and Kent [19] from 30 to 0 Myr. The long distinctive pattern of local magnetozones (N1–R5) as well as the regional stratigraphic correlation allows only one likely correlation with Mammoth to Olduvial subchron of the GPTS of Cande and Kent [19]. We considered two correlations of the magnetozones in the upper part of the Ganhangou section to the GPTS [19]. If the highest normal (N7) at the Ganhangou was correlated to the Brunhes, and N6 and sites G25 to Jaramillo and Cobb Mt subchrons respectively, the sediment accumulation rate of the upper part of the Ganhangou would be ~500 m/Myr. It is less than that of the lower parts of the section and that of the Boguzihe section. However, we did not find any evidence of decreasing sediment accumulation rates in the Ganhangou section. Given the available evidence, it is probably more realistic to assume that the sedimentation rate was constant at both sections. Because it is common to see normal overprinting on reversed sections, and given that there is only one site (G25) for the short-lived normal event in the Matuyama, we prefer to discard site G25, and correlate N7 at Ganhangou to the Jaramillo.

The two measured sections contain a total of 13 polarity zones N1–N7: 10 in the Boguzihe section (N1–N5), and seven in the Ganhangou section (N4–N7). The correlation of the local magnetostratigraphic sequences to the GPTS is best established by anchoring the distinctive long interval of normal and reversal polarity recorded in the Boguzihe and Ganhangou sections to the Gauss and Matuyama chrons, respectively (see Fig. 3).

5. Tectonic analysis of paleomagnetic directions

The expected paleomagnetic pole position for the Plio–Pleistocene at the studied area is essentially the same as the current pole position: declination = 360.0°, inclination = 58.9° for site latitude 39.7°N. The overall mean direction of tilt-corrected site-mean ChRM directions for 258 class A sites from the Boguzihe section is: declination = 349.4°, inclination = 43.2°, $k = 23.2$, $\alpha_{95} = 1.9°$ (N = 258). Using the methods of Demarest [39], a comparison of the expected and observed directions yields flattening of inclination, $F \pm \Delta F = 15.7 \pm 1.5°$, and vertical-axis rotation and error $R \pm \Delta R$ of $-10.6 \pm 2.0°$ (negative sign indicates counterclockwise).

The shallowing of the mean inclination could result from depositional shallowing of the acquired magnetization direction and/or compaction shallowing of magnetic inclination [40]. In either case, the inclination anomaly is not considered tectonically significant. In contrast, the vertical-axis rotation of declination is of tectonic significance. Although the sediments sampled from the Boguzihe section are exposed in the south limb of an anticline, apparent declination anomalies attributable to the plunge of the fold axis should be negligible according to Chan's formulation [41]. The trace of the Atushi–Talanghe anticline (where the Boguzihe section is located) sweeps clearly northward at map scale (Fig. 1). Given that the Boguzihe section is on the west side of the arch, its measured counterclockwise declination rotation of $-10.6° \pm 2.0°$ could be explained as bending of an originally straight fold-and-thrust zone in a left-stepping, sinistral, en echelon system of folds.

6. Accumulation and erosion rates, and chronology of Quaternary folding and thrusting

The relationship between the stratigraphic thickness and the magnetostratigraphic ages shows an almost linear trend in sediment accumulation rates through time, ranging in the Boguzihe section from ~800 m/Myr in the Atushi Formation to ~750 m/Myr in the Xiyu Formation (Fig. 8). Sediment accumulation rates from the Ganhangou are similar to those of the Boguzihe section (Fig. 8).

The topographic expression of the Atushi–Talanghe anticline strikes approximately northeast, and is over 100 km long, and 9 km wide (Fig. 1). The northeastern end of the anticline plunges northeast, as a northwest-verging, asymmetrical fold. In the southwest, it is an isoclinal box-like fold. The Atushi–Talanghe anticline is composed of two distinct stratigraphic sequences that are defined by a syntectonic unconformity. This syn-

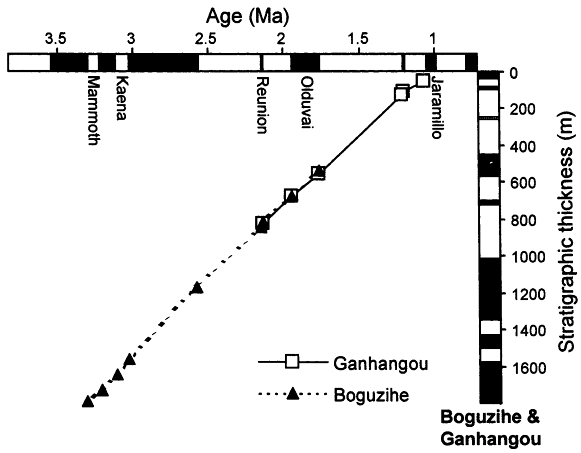

Fig. 8. Age versus stratigraphic thickness plot of the Boguzihe and Ganhangou sections using data and correlations from Fig. 3. Note that sediment accumulation rates from the Ganhangou are comparable to those of the Boguzihe section.

tectonic unconformity separates the pre-growth strata from the growth strata. The pre-growth Miocene to lower Pleistocene strata are essentially concordant, show no thickness changes and define the geometry of the anticline. In contrast, the dips of Quaternary growth strata bedding decrease rapidly across a distance of ~50 m, and show clear evidence of having developed with the growth of the Atushi–Talanghe anticline. The stratigraphic level of the syntectonic unconformity is higher in the Ganhangou section than the Boguzihe section (Figs. 2 and 3), suggesting that the initiation of folding occurs earlier in the Boguzihe section than in the Ganhangou section. The ages of this syntectonic unconformity (Fig. 3) were inferred from the accumulation rates, and indicate that folding initiated at ~1.4 Myr in the Boguzihe section, and ~1.2 Myr BP in the Ganhangou section with a rate of 30 km/Myr northeastward lateral propagation and growth of the Atushi–Talanghe anticline. Although based on the ages of growth strata at these sections, which are themselves only separated by ~6 km, this rate is strikingly consistent with the present position of the NE tip of the anticline: ~40 km NE of Ganhangou.

A cross-section was constructed by the kink-band method using dip data from field mapping at Boguzihe. Although the northern limb has poor stratigraphic control, this section appears to be parallel to the thrust transport direction (Figs. 1 and 9). An unpublished seismic section helps to define the subsurface structural geometry and clearly shows a ~9-km-deep subhorizontal decollement surface, which is interpreted to correlate with the Cenozoic basal gypsiferous unit

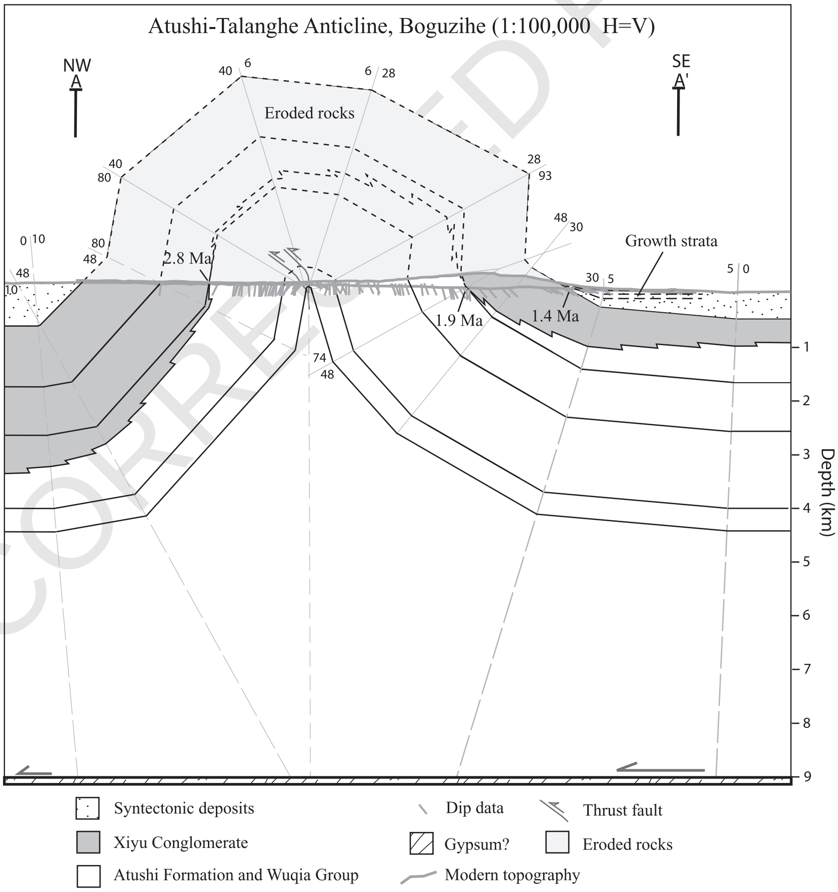

Fig. 9. Geologic cross-section of Atushi–Talanghe anticline in the Boguzihe.

documented at Aertashi, in the Southwest Tarim [28,42].

We interpret the Atushi–Talanghe anticline as a simple detachment fold (Fig. 9), due to: (1) steep limb angles (60–90°); (2) tight, box-like to isoclinal forms; (3) observed sharp kink axes accommodating changes in dip of the pre-growth strata; (4) accommodation faulting and or folding near the core of the fold, but no causal faults observed to crop out; and (5) no distinct fault ramp observable in the seismic data [43]. This interpretation maintains consistency with the seismic data, and provides a conservative estimate of total shortening of ~4.6 km and rock uplift of ~4.2 km in the Boguzihe section. In the context of the new age constraints, these estimates yield a minimum local shortening rate of ~3.3 mm/yr and an uplift rate of ~3 mm/yr. An upper limit for the total shortening is estimated by replacing the rounded top of the fold with a more box-like construction, resulting in total shortening of ~6.1 km (the rock uplift does not change). Using these values, the maximum shortening rate increases to ~4.4 mm/yr.

The geometry of the southeastern limb of the Atushi–Talanghe anticline in the Boguzihe section is well constrained by the Xiyu conglomerates (Figs. 1 and 9). Using a strict dip-domain method for reconstruction of the fold, in which the kink axis bisects the adjacent dip panels, the conglomerate contact does not connect across the fold (Fig. 9). This results from the fact that the contact is consistently 1.5–2 times closer to the core of the anticline on the northwest than on the southeast limb along strike line, suggesting that this contact is progradational, and is relatively younger on the southern limb than on the northern limb of the fold [43]. The unpublished Chinese structural maps of the Mingyaole and Kashi anticline support this interpretation. Our interpretation of the magnetic stratigraphy (Figs. 3 and 8) indicates that the age of the base of the Xiyu conglomerates in the Boguzihe section is ~1.9 Myr, obtained by interpolation between polarity chron boundaries on the southeast limb. This same boundary may be as old as ~2.8 Myr on the northwest limb, as inferred from extrapolation of similar accumulation rates to both limbs. If correct, this correlation requires a southeastward progradation rate of the Xiyu conglomerate along the Boguzihe section at ~10 km/Myr. The age of the base of the Xiyu conglomerates in the Ganhangou section is younger than ~1.0 Myr. Hence, across the ~6 km separation between the two sections, the age of the onset of conglomeratic deposition varies by about 1 Myr. It is noteworthy that, in most places, the first occurrence of major conglomeratic beds is completely unrelated to the local initiation of folding.

The growth strata partially offlap the fold limbs, so that during their deposition, the Atushi–Talanghe anticline was progressively eroded (Fig. 9). As rock uplift rates accelerated, the conglomerate-bearing river appears to have become focused into the Boguzihe location, where it has incised a suite of strath terraces that have been subsequently folded. Based on the cross-section, the maximum amount of erosion from the anticlinal crest is estimated to be 3600–3750 m. Using these data and assuming a linear erosion versus time function since the initiation of folding in the Boguzihe section (~1.4 Myr), the average erosion rate is estimated to be ~2.6–2.7 mm/yr.

7. Conclusions

Our paleomagnetic investigations of the two Plio–Pleistocene terrestrial successions provide the first detailed chronologic control for the upper Cenozoic strata in this area. Based on regional stratigraphic correlation, overall polarity pattern, and available faunal stratigraphic constraints from adjacent sections, the magnetostratigraphic section for upper part of this sequence correlates with the global magnetic polarity time scale of Cande and Kent [19] from the Mammoth subchron to the Jaramillo subchron, between 3.3 and 1.07 Myr. Sediment accumulation rates range from ~800 m/Myr in the lower part of the paleomagnetic section to ~750 m/Myr in the uppermost part of the exposed strata. The mean declination (349 ± 3°) in the Boguzihe section indicates a counterclockwise vertical-axis rotation (−11 ± 2°) during the last 1.4 Myr.

Our results show that the conglomeratic Xiyu

Formation is time-transgressive along its progradational contact with the underlying Atushi Formation. Based on magnetic correlations and extrapolated accumulation rates, the base of the Xiyu Formation ranges from less than ∼1.0 Myr in the Ganhangou section, to 1.9 Myr in the Boguzihe section to the southwest, and to ∼2.8 Myr on the northwest limb of the anticline. Thus, across a distance of ∼6 km, the initiation of conglomeratic deposition varies by ∼1 Myr. On average, the conglomeratic facies prograded southward at a rate of ∼10 km/Myr. Importantly, the onset of conglomerate deposition is not synchronous with folding.

Folding of the Atushi–Talanghe anticline initiated at ∼1.4 Myr BP in the Boguzihe section, and ∼1.2 Myr BP in the Ganhangou section, indicating a rate of 30 km/Myr northeastward lateral propagation and growth of the Atushi–Talanghe anticline. The erosion of the Atushi–Talanghe anticline crest occurred during fold growth, with an average rate of 2.6–2.7 mm/yr over the past 1.4 Myr. The cross-section in the Boguzihe provides a conservative (maximum) estimate of total shortening of about 4.6 (6.1) km and rock uplift of ∼4.2 km, yielding a conservative (maximum) shortening rate about 3.3 (4.4) mm/yr and an uplift rate of about 3 mm/yr. This rate represents about half of the geodetically determined shortening rate between the northern Tarim Basin and the Kyrgyz Tian Shan [25,26]. This result stands in contrast to the frontal thrusts in some parts of the Himalayan foreland, where analogous thrust faults and folds accommodate nearly all of the convergence between India and southern Tibet [44]. Nonetheless, this study demonstrates that the detachment folds of the SW Tian Shan play a major role in accommodating shortening along the northern margin of the Tarim Basin.

Acknowledgements

This research was supported by National Science Foundation of China Grants 49834050 and 49732090, and by the Continental Dynamics program of the US NSF (EAR 961476). J.C. is especially grateful to Prof. J.L. Kirschvink at Caltech for the use of the paleomagnetic laboratory, J.L. Kirschvink, K. Weberling, and T.D. Raub for help with the paleomagnetic technique and interpretation, Prof. Ding Guoyu and Prof. Lu Yanchou for supervising and fruitful discussions. We are grateful to Nan Ling, Tian Qinjian, Sun Dongjiang, and Ma Qia for assistance in the field. We made extensive use of software provided by Craig Jones (cjones@mantle.colorado.edu) and Li Wanlun for the analysis and presentation of paleomagnetic data. Critical and thorough reviews of an earlier draft of the manuscript by B.C. Burchfiel, S. Gilder, K.-H. Wyrwoll, and Karen Wyrwoll significantly improved the current version. This paper is China Seismological Bureau Laboratory of Geochronology and Institute of Geology contribution 2001A0003.*[SK]*

References

[1] Gansser, Geology of the Himalayas, Wiley-Interscience, New York, 1964, 289 pp.
[2] P. Tapponnier, P. Molnar, Active faulting and Cenozoic tectonics of the Tien Shan, Mongolia, and Baykal regions, J. Geophys. Res. 84 (1979) 3425–3459.
[3] J.Q. Huang, B. Chen, On the formation of molasses in the Tethys-Himalayan tectonic domain and its relation with the Indian plate motion, in: The Collection of International Geological Academic Papers, Geological Press, Beijing, 1980.
[4] Q.M. Wang, T. Nishidai, M.P. Coward, The Tarim basin, NW China; formation and aspects of petroleum geology, J. Pet. Geol. 15 (1992) 5–34.
[5] D.W. Burbank, R.A. Beck, T. Mulder, The Himalayan foreland basin, in A. Yin, T.M. Harrison (Eds.), The Tectonics of Asia, Cambridge University Press, Cambridge, 1996, pp. 205–226.
[6] P.Z. Zhang, Q.D. Deng, X.P. Yang, S.Z. Peng, X.W. Xu, X.Y. Feng, Late Cenozoic tectonic deformation and mechanism along the Tianshan Mountain, Northwestern China, Earthquake Res. China 12 (1996) 127–140.
[7] B.C. Burchfiel, E.T. Brown, Q.D. Deng, X.Y. Feng, J. Li, P. Molnar, J.B. Shi, Z. Wu, H.C. You, Crustal shortening on the margins of the Tien Shan, Xinjiang, China, Int. Geol. Rev. 41 (1999) 665–700.
[8] F. Metivier, Y. Gaudemer, Mass transfer between eastern Tien Shan and adjacent basins (Central Asia); constraints on regional tectonics and topography, Geophys. J. Int. 128 (1997) 1–17.
[9] P.Z. Zhang, P. Molnar, W.R. Downs, Increased sedimentation rates and grain sizes 2–4 Myr ago due to the influ-

ence of climate change on erosion rates, Nature 410 (2001) 891–897.
[10] N.D. Opdyke, E.H. Lindsay, G.D. Johnson, N.M. Johnson, R.A.K. Tahirkheli, M.A. Mirza, Magnetic polarity stratigraphy and vertebrate paleontology of the upper Siwalik subgroup of northern Pakistan, Palaeogeogr. Palaeoclimatol. Palaeoecol. 27 (1979) 1–34.
[11] G.D. Johnson, P. Zeitler, C.W. Nasser, N.M. Johnson, D.M. Summers, C.D. Frost, N.D. Opdyke, R.A.K. Tahirkheli, The occurrence and fission track ages of the late Neogene and Quaternary volcanic sediments, Siwalik group of Northern Pakistan, Palaeogeogr. Palaeoclimatol. Palaeoecol. 37 (1982) 63–93.
[12] D.W. Burbank, R.G.H. Raynolds, Stratigraphic keys to the timing of deformation: an example from the northwestern Himalayan foredeep, in: C. Paola, K. Kleinspehn (Eds.), New Perspectives in Basin Analysis, Springer-Verlag, New York, 1988, pp. 331–351.
[13] N. Brozovic, D.W. Burbank, Dynamic fluvial systems and gravel progradation in the Himalayan foreland, Geol. Soc. Am. Bull. 112 (2000) 394–412.
[14] T. Ojha, R.F. Butler, J. Quade, P.G. DeCelles, D. Richards, B.N. Upreti, Magnetic polarity stratigraphy of the Neogene Siwalik Group at Khutia Khola, far western Nepal, Geol. Soc. Am. Bull. 112 (2000) 424–424.
[15] H. Chen, X.L. Lin, K.N. Guan, J.M. Xu, Early Pleistocene deposits and its lower boundary (Q/N) in Tian Shan MT, Xinjiang Region, Quat. Sci. 1 (1994) 38–47.
[16] Z.H. Teng, L.P. Yue, R.H. Pu, X.Q. Deng, X.W. Bian, The magnetostratigraphic age of the Xiyu Formation, Geol. Rev. 42 (1996) 481–489.
[17] J.H. Yin, S. Nie, P. Craig, T.M. Harrison, Late Cenozoic tectonic evolution of the southern Chinese Tian Shan, Tectonics 17 (1998) 1–27.
[18] H.B. Zheng, C.M. Powell, Z.S. An, J. Zhou, G.R. Dong, Pliocene uplift of the northern Tibetan Plateau, Geology 28 (2000) 715–718.
[19] S.C. Cande, D.V. Kent, Revised calibration of the geomagnetic polarity timescale for the Late Cretaceous and Cenozoic, J. Geophys. Res. 100 (1995) 6093–6095.
[20] Xinjiang Bureau of Geology and Mineral Resources (XBGMR), Geological map of southwestern Xinjiang, scale 1:500 000, 1985.
[21] G.P. Wang, G.T. Wu, Z.Q. Lun, Y.Y. Zhu (Eds.), Regional Geology of Xinjiang Uygur Autonomous Region, Bureau of Geology and Mineral Resources of Xinjiang Uygur Autonomous Region, Geological Memoirs Series 1: Geological Publishing House, Beijing, 1993, 841 pp.
[22] M.B. Allen, S.J. Vincent, P.J. Wheeler, Late Cenozoic tectonics of the Kepingtage thrust zone: Interactions of the Tien Shan and Tarim Basin, Northwest China, Tectonics 18 (1999) 639–654.
[23] D.S. Li, D.G. Liang, C.Z. Jia, G. Wang, Q.Z. Wu, D.F. He, Hydrocarbon accumulations in the Tarim basin, China, Am. Assoc. Pet. Geol. Bull. 80 (1996) 1587–1603.
[24] J. Chen, G.S. Qu, J. Shen, E. Sobel, L. Nan, Q.J. Tian, J.H. Yin, Late Cenozoic tectonics along the northwestern margin of the Tarim basin: Interactions between the Tarim basin and the southern Tian Shan, west China. Abstracts of 15th Himalaya-Karakoram-Tibet Workshop, Chengdu, China, Earth Sci. Front. 7 (Suppl.) (2000) 323–325.
[25] Q. Wang, G.Y. Ding, X. Qiao, X.Q. Wang, Research on present crustal deformation in the southern Tian Shan (Jiashi), China by GPS geodesy, Acta Seismol. Sin. 22 (2000) 263–270.
[26] Ch. Reigber, G.W. Michel, R. Galas, D. Angermann, J. Klotz, J.Y. Chen, A. Papschev, R. Arslanov, V.E. Tzurkov, M.C. Ishanov, New space geodetic constraints on the distribution of deformation in Central Asia, Earth Planet. Sci. Lett. 191 (2001) 157–165.
[27] J. Chen, J.H. Yin, G.S. Qu, K.Q. Zhang, Timing, lower boundary, genesis, and deformation of the Xiyu Formation around the western margins of the Tarim Basin, Seismol. Geol. 22 (Suppl.) (2000) 104–116.
[28] Z.Y. Zhou P.J. Chen, Biostratigraphy and Geologic Evolution: Petroleum Geology of Tarim Basin, Science Press, Beijing, 1990, 439 pp.
[29] L.Y. Hu, Late Tertiary foraminifera of Tarim Basin and their geological significance, Chin. Sci. Bull. 15 (1982) 938–941.
[30] Chinese Bureau of Geology, Stratigraphic Tables for Xinjiang Autonomous Region, Geological Publishing House, Beijing, 1981, 496 pp.
[31] P. Molnar, E.T. Brown, B.C. Burchfiel, Q.D. Deng, X.Y. Feng, J. Li, G.M. Raisbeck, J.B. Shi, Z.M. Wu, F. Yipu, H.C. You, Quaternary climate change and the formation of river terraces across growing anticlines on the north flank of the Tien Shan, China, J. Geol. 102 (1994) 583–602.
[32] P.A. Allen, J.D. Collinson, Lakes, in: H.G. Reading (Ed.), Sedimentary Environments and Facies, Blackwell Scientific, Oxford, 1986, pp. 63–94.
[33] R.A. Fisher, Dispersion on a sphere, Proc. R. Soc. London A 217 (1953) 295–305.
[34] P.L. McFadden, M.W. McElhinny, The combined analysis of remagnetization circles and direct observations in paleomagnetism, Earth Planet. Sci. Lett. 87 (1988) 161–172.
[35] J.L. Kirschvink, The least-squares method line and plane and the analysis of palaeomagnetic data, Geophys. J. R. Astron. Soc. 62 (1980) 699–718.
[36] G.S. Watson, A test for randomness of directions, R. Astron. Soc. Geophys. J. Mon. Not. 7 (1956) 160–161.
[37] P.L. McFadden, M.W. McElhinny, Classification of the reversal test in paleomagnetism, Geophys. J. Int. 103 (1990) 725–729.
[38] P.L. McFadden, D.L. Jones, The fold test in paleomagnetism, Geophys. J. R. Astron. Soc. 67 (1981) 53–58.
[39] H.H. Demarest Jr., Error analysis for the determination of tectonic rotation from paleomagnetic data, J. Geophys. Res. 88 (1983) 4321–4328.
[40] S. Gilder, Y. Chen, S. Sen, Oligo-Miocene magnetostratigraphy and rock magnetism of the Xishuigou section,

Subei (Gansu Province, western China) and implications for shallow inclinations in central Asia, J. Geophys. Res. 106 (2001) in press.

[41] L.S. Chan, Apparent tectonic rotations, declination anomaly equations, and declination anomaly charts, J. Geophys. Res. 93 (1988) 12151–12158.

[42] E.R. Sobel, T.A. Dumitru, Thrusting and exhumation around the margins of the western Tarim basin during the India-Asia collision, J. Geophys. Res. 102 (1997) 5043–5063.

[43] K. Scharer, D.W. Burbank, J. Chen, C. Rubin, R.B. Zhao, Quaternary folding of Cenozoic strata along the southwestern margin of the Tien Shan, China, Annual Geological Society of America Meeting Abstracts, 2000.

[44] J. Lavé, J.P. Avouac, Active folding of fluvial terraces across the Siwalik Hills, Himalaya of central Nepal, J. Geophys. Res. 105 (2000) 5735–5770.